Ferromagnetic epitaxial Cr_2O_3 thin films grown on oxide substrates by Pulsed Laser Deposition

María Vila[a,b,*], Juan Rubio – Zuazo[a,b], Irene Lucas[c,d], César Magén[c,d], Alicia Prados[e], Eduardo Salas-Colera[a,b,f] , Icíar Arnay[a,b] and Germán Rafael Castro[a,b]

[a]*SpLine CRG BM25 Beamline, The European Synchrotron, 71, Avenue des Martys, 38000 Grenoble, France*

[b]*Instituto de Ciencia de Materiales de Madrid, Consejo Superior de Investigaciones Científicas (ICMM-CSIC), 28049 Madrid, Spain*

[c]*Instituto de Nanociencia y Materiales de Aragón (INMA), CSIC-Universidad de Zaragoza, Zaragoza 50009, Spain*

[d]*Departamento de Física de la Materia Condensada, Universidad de Zaragoza, Zaragoza 50009, Spain*

[e]*Departamento de Física de Materiales, Facultad de Ciencias Físicas, Universidad Complutense de Madrid, 28040 Madrid, Spain*

[f]*Departamento de Física, Escuela Politécnica Superior, Universidad Carlos III de Madrid (UC3M), 28911, Leganés, Madrid, Spain*

**Corresponding author: María Vila, Current address: IMDEA Materiales, C/Eric Kandle, 2, 28906, Getafe, Madrid. maria.vila@imdea.org*

Abstract

Single-phase and single-oriented epitaxial Cr_2O_3 thin film has been grown on $SrTiO_3$ (111) substrate for the first time. The morphology, epitaxial growth mode and oxygen stoichiometry of the obtained film have been investigated by AFM, XRR, XRD and XPS, and compared to thin film grown on α-Al_2O_3 under equivalent conditions. The $Cr_2O_3/SrTiO_3$ system presents a non - coincidence growth based on in – plane rotation of 30° of the Cr_2O_3 layer respect to the underlying $SrTiO_3$ (111) substrate, while a coincidence growth based on axis-on-axis coupling is present for

Cr_2O_3/α-Al_2O_3. However, in both cases an in-plane compression occurs in order to match the layer and substrate lattices. The formation of punctual defects in the form of oxygen vacancies have been observed by XPS for the layer grown on α-Al_2O_3, being the main mechanism for strain alleviation (-4%). However, the 18 nm thick layer grown on $SrTiO_3$ presents stoichiometric oxygen content maintaining an epitaxial strain (-1.6%) accumulated on the lattice. Both epitaxial Cr_2O_3 layers show soft ferromagnetic response with coercive fields of 60 Oe and 90 Oe for the layer grown on $SrTiO_3$ and α-Al_2O_3, respectively.

Keywords

Thin films, Pulsed Laser Deposition, Surface X – Ray Diffraction, Antiferromagnetic oxide

1. Introduction

Chromium trioxide (Cr_2O_3) is a widely studied oxide, being an important technological material because of its intrinsic properties. It is an antiferromagnetic (AFM, Néel Temperature (T_N) = 307 K) and the first discovered magnetoelectric material above room temperature [1-3]. Bulk Cr_2O_3 also presents uniaxial magnetic anisotropy along the [111] direction. Additionally, it is a good insulator. The combination of these properties makes this material suitable as a building block in different technological devices. In particular, Cr_2O_3 has been employed in devices which involve exchange bias effect of coupled ferromagnetic - antiferromagnetic systems [1]. Furthermore, as a result of its good insulating properties, it is also suitable for magnetic tunnel junctions [2]. Cr_2O_3 is a potential candidate for heteroestructures based on epitaxial thin films as it can be easily prepared using a simple growth process. For instance, it has been already implemented as a buffer layer for the growth of other thin films, and has been employed as anode material for Li – ion batteries. However, special attention should be paid to the modification of its

intrinsic properties due to the accumulated epitaxial strain. Previous results revealed that the presence of strain induces defects, such as oxygen vacancies, which can infer dramatic changes of its magnetic properties. For instance, unexpected ferromagnetism was found to occur in highly strained Cr_2O_3 thin films [3,4]. Also, an enhancement of T_N has been directly related to in–plane lattice contraction [5]. Thus, the ability of Cr_2O_3 to tune its intrinsic properties by artificial strain through epitaxial growth opens the way to the development of complex technological devices. For that, it is mandatory to explore the use of new substrates as templates for the epitaxial growth of Cr_2O_3 thin films with exotic macroscopic response. Several substrates have been already used, such as sapphire (α - Al_2O_3) [6,7], graphene [8], Co [9], garnet [10], Cr (110) [11], $YAlO_3$ (001) [12], TiO_2 [13],$LiNbO_3$(0001) [14] or Ni(111) with a graphene buffer [15]. However, the use of the well-known $SrTiO_3$ (STO) substrate has been scarcely explored. An attempt of epitaxial growth has been achieved on STO (001) using CeO_2 as buffer layer [16]. However, direct growth of Cr_2O_3 on STO surface has not been reported yet. The successful epitaxial growth directly on $SrTiO_3$ is of special importance as this material has been widely used for applications in microelectronics due to its high charge storage capacity, chemical stability and its excellent insulating properties [17,18]. Hence, the combination of Cr_2O_3 and STO intrinsic properties provides a unique possibility to obtain different macroscopic responses on the same heterostructure. In the present work we have successfully grown for the first time epitaxial Cr_2O_3 thin films on STO (111) substrates. A complete morphological, structural, electronic and magnetic characterization is presented based on a comparison with epitaxial thin films grown on sapphire using equivalent conditions.

2. Experimental section

Cr_2O_3 thin films were grown on $SrTiO_3$(111) and α - Al_2O_3(0001) substrates (5x5 mm^2) by Pulsed Laser Deposition (PLD). A Nd:YAG laser (λ = 355 nm) with 10 Hz and 1 J/cm^2 irradiance power was used to ablate a polycrystalline Cr metal target. The deposition was carried out in an oxygen atmosphere of 10^{-4} mbar and at a surface temperature of 350 °C. High surface crystallinity was determined by in-situ Reflection High-Energy Electron Diffraction (RHEED) using a primary electron beam of 29 keV. The topography of the samples has been studied by means of a multimode Nanoscope IIIa Atomic Force Microscope (Bruker) with a Si tip (Bruker, model TESP), working in tapping mode and operating in air. Images of different sizes were analyzed with WSxM 5.0 software[19] .

The structural characterization of the Cr_2O_3 thin films in both $SrTiO_3$ (111) and α – Al_2O_3 (0001) was investigated by means of High Resolution Grazing Incidence X-ray Diffraction (HR-GIXRD) in BM25B - SpLine beamline at the ESRF [20]. This end station is composed of a six-circle multipurpose diffractometer in vertical geometry. A photon energy of 15 keV (λ = 0.826 Å) was used during the experiment to ensure the access to a wide reciprocal space region. Special attention was paid to the study of the growth mechanism of the thin films in the two different substrates, to understand the coupling of the layers lattice with respect to the substrate lattice, as well as to elucidate the possible presence of compressive or tensile stress in the grown films. A layer thickness in the tens of nanometer range, compatible with device manufacturing, in which the epitaxial character still plays an important role but size effects due to ultra-short thicknesses are ruled out has been used for this study. Information about the Cr valence and oxygen stoichiometry was obtained using X-ray Photoelectron Spectroscopy (XPS) methods on the Cr 3s core level using a standard monochromatic X-ray tube, with a Mg K_α radiation anode (hν = 1253.6 eV)..

Scanning Transmission Electron Microscopy (STEM) images of the films were performed in High Angle Annular Dark Field (HAADF) mode using a FEI Titan 60-300 equipped with an aberration corrector for the probe. The convergence angle used was 24 mrad to provide a spatial resolution below 0.1 nm.

The magnetic characterization was performed by Superconducting Quantum Interference Devices (SQUID) Magnetometer at room temperature under a maximum field of 5 T.

3. Results and Discussion

During the thin film growth by PLD, in-situ RHEED was used to monitor the evolution of the layers crystallinity. Fig. 1a-d shows representative RHEED patterns of the clean substrates, STO (111) and α - Al_2O_3 (0001) (Fig. 1a and c), and the evaporated Cr_2O_3 layers (Fig. 1b and d). The RHEED patterns show smooth diffraction stripes, representative of a smooth, homogeneous and crystalline layer. The morphology of the film surface of the different samples has been studied by AFM. Fig. 2a and b show the topography of the Cr_2O_3 thin films grown on $SrTiO_3$ and α-Al_2O_3, respectively. In both cases a good layer coverage and homogeneity is obtained. AFM profile measurements performed along the surface reveal a flat surface, with root mean square (rms) roughness of approximately 1 nm for the layer grown on $SrTiO_3$ (Fig. 2c). Cr_2O_3/Al_2O_3 films show isolated islands on top of a homogeneous coverage. Profile measurements (Fig. 2d) show rms roughness values of 3 – 4 nm. A similar behavior is obtained from synchrotron-based X-ray reflectivity (XRR) measurements (Fig. 2e and f). Intense Kiessig fringes are observed for the $Cr_2O_3/SrTiO_3$ sample, despite the nearly identical densities for the layer (5.22 g/cm^3) and substrate

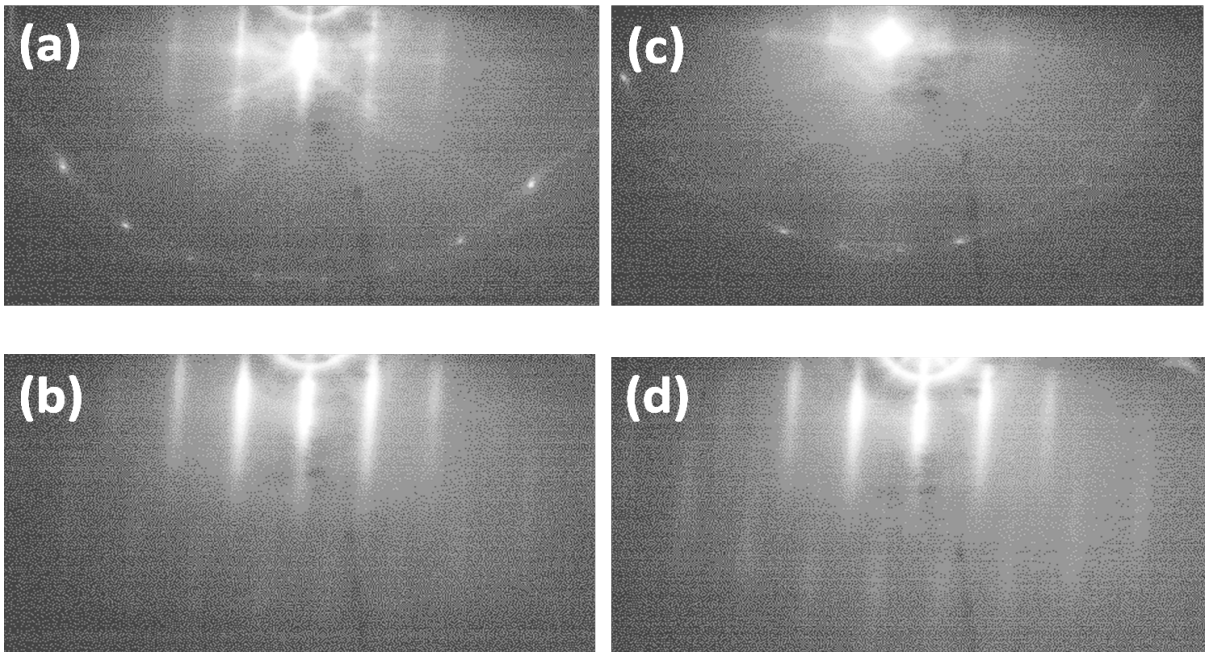

Figure 1. RHEED patterns of the clean Al_2O_3 (0001) substrate (a) and (b) the Cr_2O_3 thin layer. (c) and (d) images show RHEED patterns for the $SrTiO_3$ substrate and deposited Cr_2O_3 film.

(5.12 g/cm^3), indicating the presence of abrupt interfaces and flat surfaces, while for the Cr_2O_3/α-Al_2O_3 sample the rapid attenuation of Kiessig fringes indicates the presence of a rough surface. Also based on the isostructural character between Cr_2O_3 and α-Al_2O_3, chemical substitution at the interface is more than probable, which will contribute to the absence of well-defined XRR interference. Thickness values of 18.2(3) nm and 17.7(6) nm have been obtained for the layer grown on $SrTiO_3$ and α-Al_2O_3, respectively from the reflectivity curves.

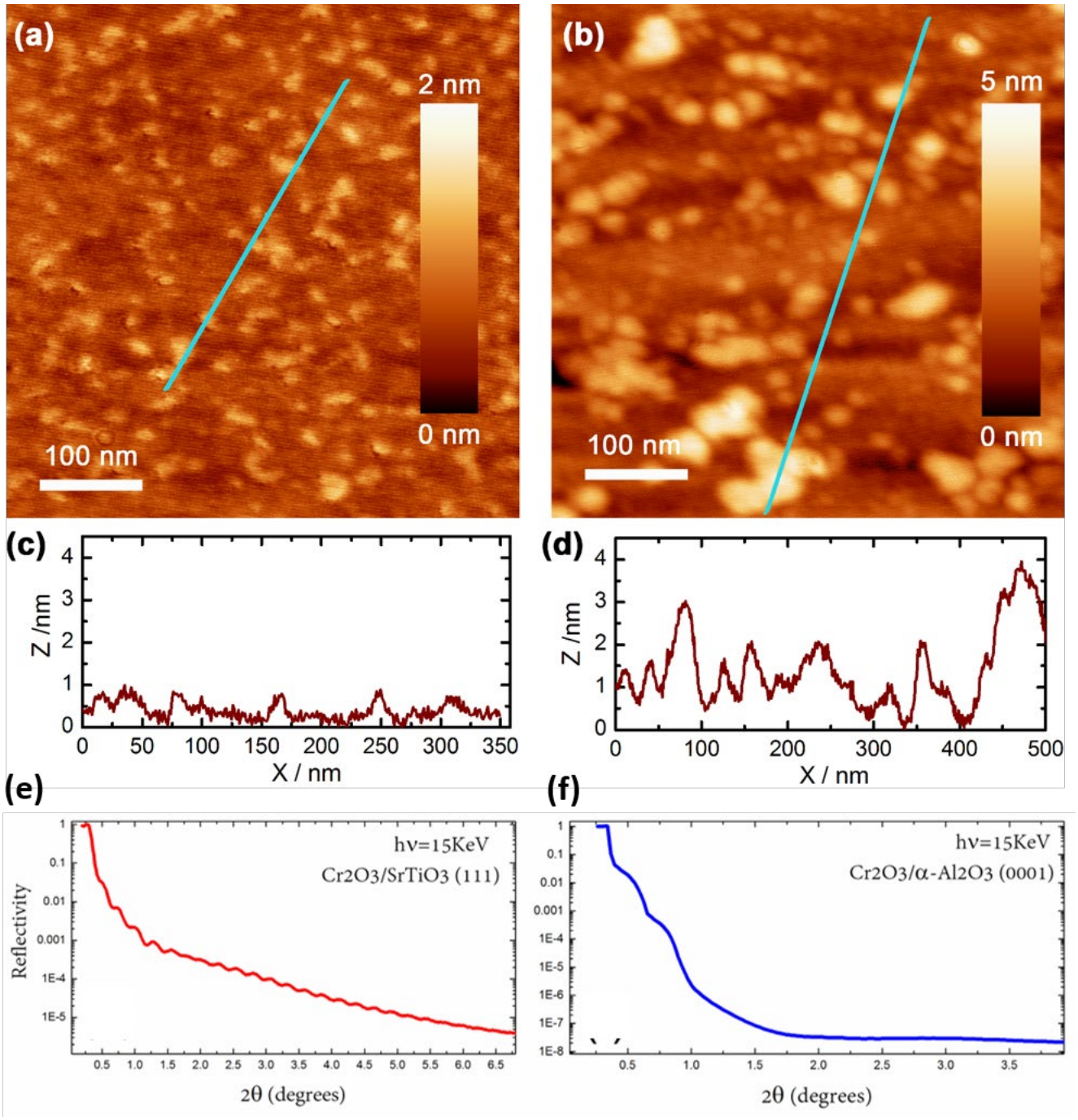

Figure 2. AFM images (0.5 x 0.5 μm) of Cr_2O_3 thin films grown on a) $SrTiO_3$ and b) α-Al_2O_3. c) and d) are the AFM profiles measured in the marked lines in a) and b), respectively. e) and f) show X-ray reflectivity curves for the layers grown on $SrTiO_3$ and α-Al_2O_3, respectively.

Bulk sapphire (α-Al_2O_3) (corundum structure) presents in-plane and out-of-plane lattice parameter values of a = b = 4.76 Å and c = 12.99 Å, respectively [21]. In the case of Cr_2O_3, isostructural with sapphire, lattice parameters are a = b = 4.96 Å and c = 13.59 Å. The in-plane lattice mismatch with respect to Cr_2O_3 is - 4.2% which favors the epitaxial coupling between both lattices. However, $SrTiO_3$ on the (111) orientation, presents lattice parameters of a = b = 5.5225 Å and c = 6.76 Å implying a lattice mismatch of +10.2% with Cr_2O_3, being unfavorable for a coincidence growth. To understand the in-plane coherence between the layers and substrates lattices High Resolution XRD and Reciprocal Space Maps (RSM) measurements were performed. Fig. 3a shows, for the $Cr_2O_3/SrTiO_3$ system, the RSM around the (202) diffraction peak of the $SrTiO_3$. It can be clearly seen that the diffraction peaks maxima corresponding to the Cr_2O_3 layer and the $SrTiO_3$ substrate have different in-plane values. Peaks corresponding to STO are those present along the marked yellow line in the figure (H = 2), while two peaks associated to the Cr_2O_3 thin film are aligned along H = 1.96 (red line). This XRD pattern can be explained by a non – coincidence epitaxial growth in which the in-plane lattice of the single oriented Cr_2O_3 (0001) rotates 30^0 respect to the underlying $SrTiO_3$ (111) plane in order to reduce the lattice mismatch minimizing the epitaxial energy. Such a lattice coupling has been already reported for other transition metal oxides (TM_2O_3) grown on $SrTiO_3$ (111), for instance for α-Fe_2O_3 [22]. Calculations performed in different diffraction peaks reveal Cr_2O_3 in – plane lattice parameters of 4.88(4) Å. The difference, in comparison to reported Cr_2O_3 bulk values (a = b = 4.96 Å), results in a compressive strain of -1.6 %. Hence, although a non – coincidence growth is present the Cr_2O_3 layer is strained to match the $SrTiO_3$ lattice. Fig. 3c shows a diagram on the real-space of the Cr_2O_3 in-plane lattice respect to the substrate lattice in which it can be seen that nearly a perfect coupling between both lattices occurs due to the layer lattice rotation. Out-of-plane scans along the in-plane

values for $SrTiO_3$ (Crystal Truncation Rod (CTR) yellow line in the RSM) and Cr_2O_3 (ROD, red line in the RSM) reveal high surface signal between Bragg peaks (Fig. 3b and c) indicating the presence of flat and sharp surface and interface, in agreement with the AFM and XRR measurements. The out-of-plane lattice parameter for Cr_2O_3 increases to c = 14.03(3) Å respect to the bulk value (c = 13.59 Å) maintaining the volume of the bulk unit cell.

In the case of the Cr_2O_3 layer grown on α-Al_2O_3 (0001), as the former is known to be isostructural to the latter, an axis-on-axis (coherent) growth is expected. Fig. 3d shows the corresponding RSM around the (116) reflection of α-Al_2O_3 (0001) in which it can be seen that the diffraction peak from the Cr_2O_3 and α-Al_2O_3 has the same in-plane momentum transfer revealing an axis-on-axis coincidence epitaxial growth. The Cr_2O_3 shrinks its lattice in order to match its in-plane lattice parameter with that of the substrate (a = b = 4.76 Å) as shown in the diagram of Fig. 3g. The coincidence growth induces a compressive strain of -4% to the Cr_2O_3 lattice. In the out-of-plane direction the Cr_2O_3 lattice is expanded to c = 14.18(4) Å. In contrast to the layer grown on STO the unit cell volume is not preserved being reduced by 4%. Such a volume reduction reflects the possible presence of a large number of point defects produced by the coincidence growth, in the form of oxygen vacancies or Al/Cr chemical substitution. High resolution GIXRD scans along the out-of-plane direction (CTR) have been measured revealing the absence of surface signal between Bragg peaks, as shown in Fig. 3e. Such a behavior indicates the presence of a rough surface and buried interface, in agreement with the AFM and XRR measurements.

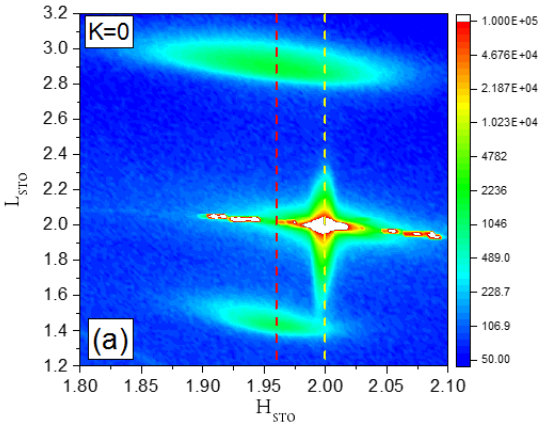
K=0
(a)
L_{STO}
H_{STO}

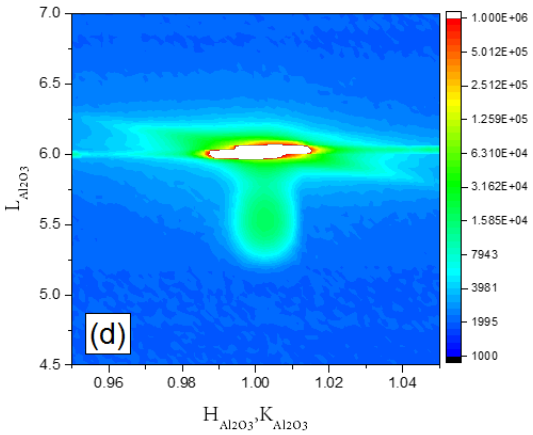
(d)
L_{Al2O3}
H_{Al2O3},K_{Al2O3}

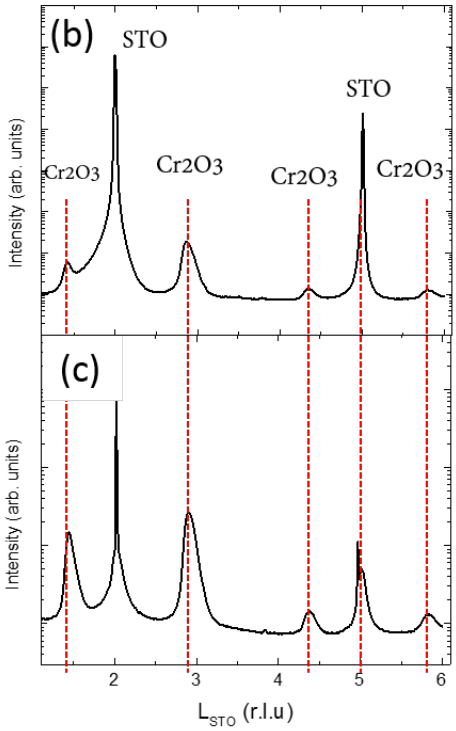
(b)
STO
STO
Cr2O3
Cr2O3
Cr2O3
Cr2O3
(c)
Intensity (arb. units)
Intensity (arb. units)
L_{STO} (r.l.u)

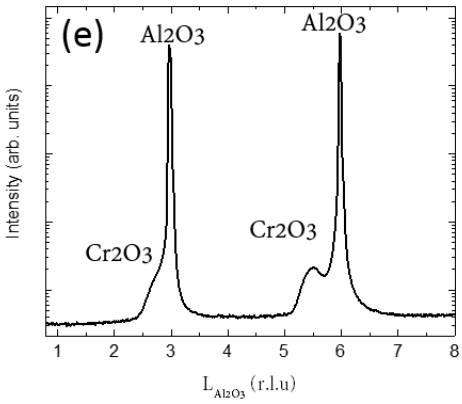
(e)
Al2O3
Al2O3
Cr2O3
Cr2O3
Intensity (arb. units)
L_{Al2O3} (r.l.u)

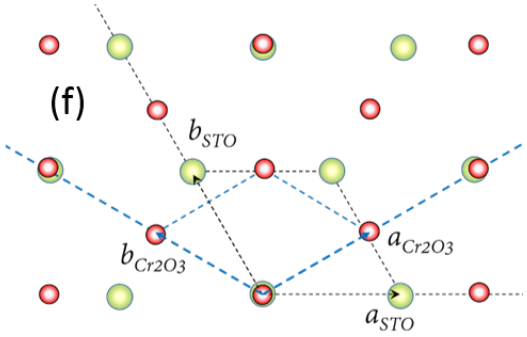
(f)
b_{STO}
b_{Cr2O3}
a_{Cr2O3}
a_{STO}

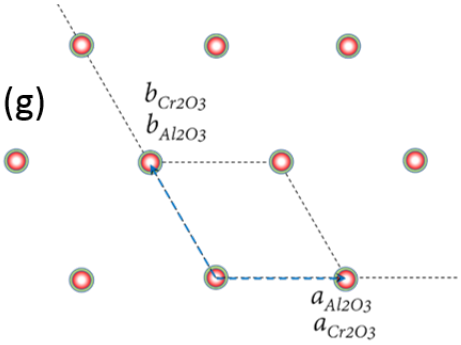
(g)
b_{Cr2O3}
b_{Al2O3}
a_{Al2O3}
a_{Cr2O3}

Figure 3. (a) (H vs L) reciprocal space map at K = 0 for Cr_2O_3 thin film (marked with a red dashed line) grown on STO(111) (yellow dashed line). Different in-plane values are obtained for Cr_2O_3 and $SrTiO_3$ revealing an epitaxial non - coincidence growth. (b) CTR and (c) ROD for the layer grown on $SrTiO_3$. Flat surface and interface are inferred from the surface signal present between the layers Bragg peaks; (d) (H = K vs L) reciprocal space map for Cr_2O_3 thin film grown on α-Al_2O_3. Identical in-plane values are obtained for Cr_2O_3 and α-Al_2O_3 revealing an epitaxial coincidence growth; (e) CTR for the layer grown on α-Al_2O_3. The absence of surface signal reveals the presence of rough surface and interface; Layer and substrate lattice diagrams in real space showing the in-plane coupling for Cr_2O_3 layers grown on (f) $SrTiO_3$ and (g) α-Al_2O_3.

In-plane rocking scans at different Cr_2O_3 reflections have been performed to evaluate the crystallographic domain sizes. Extremely large domain sizes of 140(1) nm are present for the layer grown on α-Al_2O_3, while moderate domain sizes of 8(1) nm are obtained for the layer grown on $SrTiO_3$. The coincidence growth on α-Al_2O_3, compared to the non - coincidence growth on $SrTiO_3$, favors the formation of crystals with larger domains. As revealed by the unit cell volume modification, the alleviation of the accumulated stress via the formation of punctual defects on the layers grown on α-Al_2O_3 favors even more the formation of large size domains.

STEM images evidence the epitaxial growth of Cr_2O_3 on both substrates. On α-Al_2O_3 the growth is fully coherent (Fig. 4a), with a sharp defect free interface, as expected from a film that presents naturally the same crystal symmetry as the substrate. In the case of the STO film (Fig. 4b), the different crystal structures of film and substrate prevent the coherent growth. The epitaxy relations between film and substrate are STO (111)[1-10] // Cr_2O_3 (0001)[1-120] in agreement with the XRD results. A highly defective layer is clearly observed at the interface, as a result of the

huge lattice mismatch. Figure 4(b) show contrast differences which in these systems are associated to planar crystallographic domains, antiphase domains (APD). The possibility of studying punctual defects, such as oxygen vacancies, is not possible due to the complex microstructure of these systems.

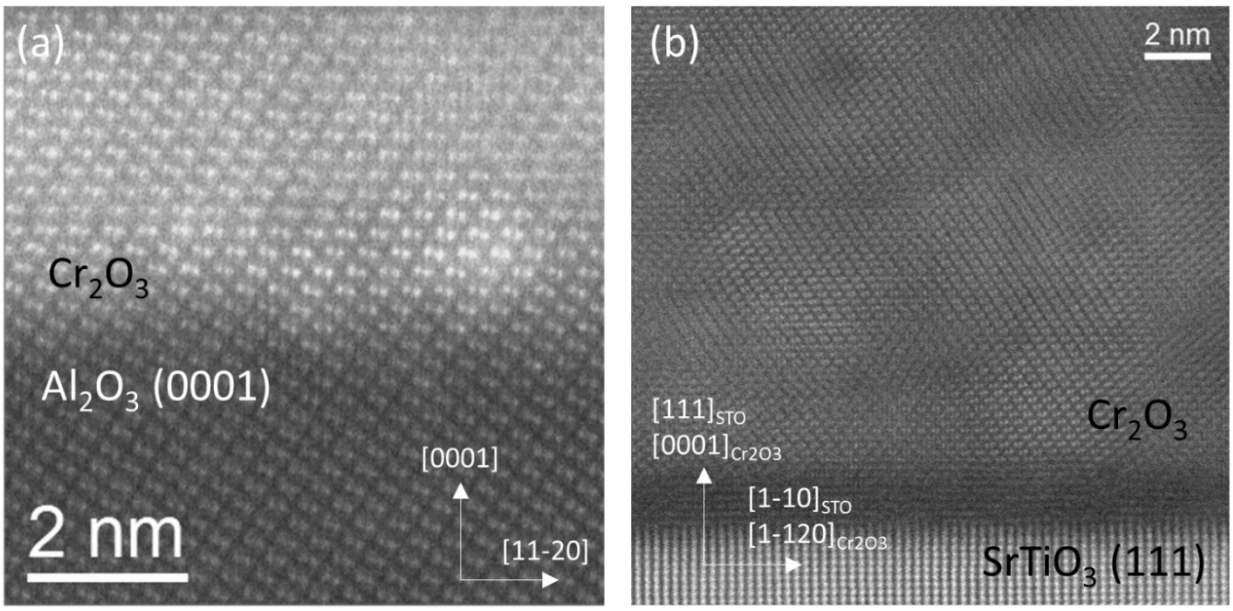

Figure 4. HAADF-STEM images of the Cr_2O_3 films grown on (a) α-Al_2O_3 (0001) and (b) $SrTiO_3$ (111). The epitaxy relations between the films and their respective films are indicated.

XPS measurements on the Cr 3s core level have been made to assess the oxidation state of Cr and elucidate and quantify the presence of punctual defects in the form of oxygen vacancies on the surface and sub-surface region (Fig. 5). The XPS spectra for 3s core level in transition metals is characterized by a splitting which is originated from the exchange coupling between the 3s hole and the 3d electrons. The magnitude of the splitting is dependent on the chemical state [23–25]. In the case of most transition metals, as for instance for Cr compounds, a linear relationship between

3s splitting and oxidation state is expected [26]. In the case of stoichiometric Cr_2O_3 with formal Cr valence of +3 an energy splitting of 4.1 eV has been reported [27] which coincides with the splitting found for other Cr(III) compounds. Larger splitting values of 5.2 eV has been reported for Cr^{+2} compounds [28] while lower values of 3.5 eV has been found for Cr^{+4} compounds [25]. Fig. 5 shows the Cr 3s XPS spectra obtained in the present work in which the splitting is clearly resolved. The spectra have been aligned to the 3s main peak in order to clearly identify differences in the energy splitting. Slightly different energy splitting is obtained for each sample indicating the presence of faint differences in the Cr oxidation state. An energy splitting of 4.07(4) eV corresponding to a Cr^{+3} valence is obtained for the sample grown on $SrTiO_3$ indicating the presence of stoichiometric Cr_2O_3 phase. In contrast, larger energy splitting of 4.35(4) eV is obtained for the sample grown on α-Al_2O_3 corresponding to a lower Cr oxidation state of +2.75. Hence, the formation of 8% oxygen vacancies occurs in the chromium oxide lattice ($Cr_2O_{3-\delta}$ with δ=0.25) in order to release the strain induced by the epitaxial coincidence growth. An increase of the out-of-plane lattice parameter is then expected in agreement with the results obtained by XRD. From the XPS Cr 3s spectra it can be also seen that the energy width of the satellite peak (higher binding energy) for the layer grown on α-Al_2O_3 is larger than expected. A value of 2.7 eV is obtained while similar values (2.2 eV at FWHM) for the main and satellite peak should happen [27,28], as is the case of the layer grown on $SrTiO_3$. The broadening of the satellite peak for the layer grown on α-Al_2O_3 is indicative of the presence of extra interactions with the oxygen ligands that creates extra final states and hence extra satellite structure [29], probably linked to the presence of punctual defects in the form of oxygen vacancies. The experimental integrated intensity of the satellite peak is however very similar for both systems giving rise to nearly equal ratio of intensity of the multiplet peaks for each system. In a simple scenario the intensity ratio of the Cr 3s peaks is

dependent on the spin multiplicitites [30]. In the case of the Cr_2O_3 due to the $3d^3$ high spin configuration of the Cr^{+3} ion with $S_{3d} = 3/2$ the intensity ratio is then given by I (3d ↑↑↑ 3s ↑) : I (3d ↑↑↑ 3s ↓) = S_{3d} + 1 : S_{3d} = 5:3, while for the Cr^{+2} ion the intensity ratio is given by 3:2. In the case of a $Cr^{+2.75}$ the ratio is then of 5:3.08 in accordance with the experimental behavior obtained from the measurements.

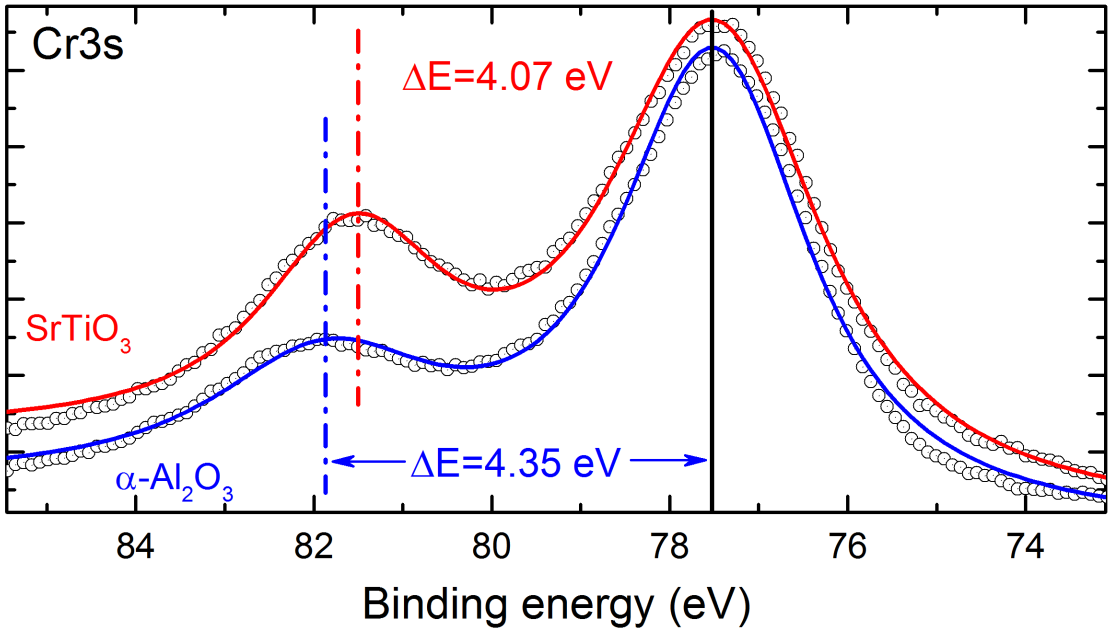

Figure 5. XPS measurements on the Cr 3s core level. A larger energy splitting is obtained for the layer grown on α-Al_2O_3 (blue curve) revealing a reduction of the Cr oxidation state as compared to the layer grown on $SrTiO_3$ (red curve). Both spectra have been aligned on the main 3s peak in order to clearly show the difference in energy splitting.

Fig. 6a shows the measured magnetic response of the studied samples. Both samples show single phase hysteresis loops with very similar coercive field. 60 Oe when deposited on α-Al_2O_3, and 90 Oe when deposited on $SrTiO_3$ (Fig. 6b and inset). Nevertheless, in the case of the layer grown on $SrTiO_3$ the measured remanence is the double than in the case of the layer deposited on sapphire, maybe due to the energy lost at expenses of rotating domains. These results are consistent with the

observed domain size in every sample (140 nm and 8 nm for layers grown on α-Al_2O_3 and $SrTiO_3$, respectively). The ferromagnetic response can be attributed to the strain accumulated because of the epitaxial growth, as previously reported [3,4]. In the case of the layer grown on $SrTiO_3$, even if a non – coincidence growth occurs, a remaining strain of -1.6% has been experimentally observed inducing the ferromagnetic behavior.

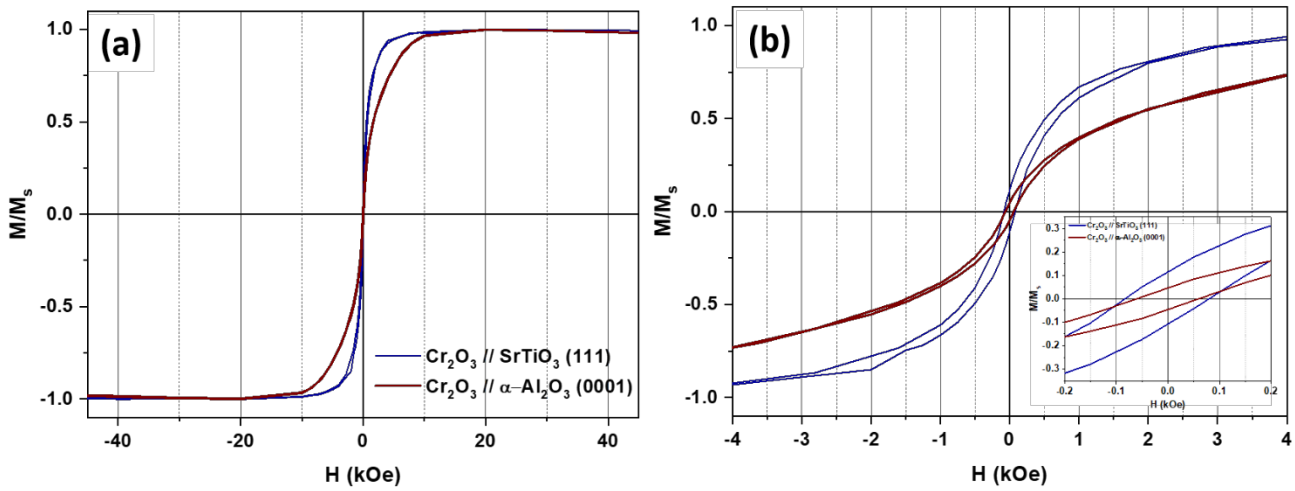

Figure 6. Comparison of normalized magnetization hysteresis loops of Cr_2O_3 thin films measured at 300 K on α - Al_2O_3 and $SrTiO_3$. (a) Complete hysteresis loops up to 50 kOe showing the correct magnetic saturation of the samples (b) Zoom of the hysteresis loops to better compare remanence and coercive fields in every sample.

CONCLUSIONS

The successful epitaxial growth of single phase and single oriented Cr_2O_3 thin films on $SrTiO_3$ (111) has been achieved for the first time. We demonstrate that the use of $SrTiO_3$ (111) substrate is favourable for the growth of high quality Cr_2O_3 epitaxial thin films. Low surface

roughness and absence of oxygen vacancies are found for the layer grown on $SrTiO_3$ while a moderately rough surface coupled to the presence of oxygen defects is found for the layer grown on α - Al_2O_3 (0001). However larger crystallographic domain sizes of 140 nm resulted from the coincidence growth on the α-Al_2O_3(0001) substrate compared to the moderate values of 8 nm obtained for the layer grown in a non - concidence way on $SrTiO_3$ (111). Nevertheless the domain sizes obtained for both systems are compatible with nowadays technological requirements. Soft ferromagnetic response has been obtained in both epitaxial layers with very similar coercive field being slightly higher for the layer grown on $SrTiO_3$. Ferromagnetic epitaxial Cr_2O_3 grown on oxide substrates becomes a potential candidate for the development of complex magnetic based devices.

References

[1] X.H. Liu, W.B. Cui, X.K. Lv, W. Liu, X.G. Zhao, D. Li, Z.D. Zhang, Exchange bias in antiferromagnetic coupled Fe $_3$ O $_4$ +Cr $_2$ O $_3$ nanocomposites, J. Phys. D. Appl. Phys. 41 (2008) 105005. https://doi.org/10.1088/0022-3727/41/10/105005.

[2] R. Cheng, C.N. Borca, N. Pilet, B. Xu, L. Yuan, B. Doudin, S.H. Liou, P.A. Dowben, Oxidation of metals at the chromium oxide interface, Appl. Phys. Lett. 81 (2002) 2109–2111. https://doi.org/10.1063/1.1506942.

[3] S. Punugupati, J. Narayan, F. Hunte, Strain induced ferromagnetism in epitaxial Cr2O3 thin films integrated on Si(001), Appl. Phys. Lett. 105 (2014) 2012–2017. https://doi.org/10.1063/1.4896975.

[4] S. Punugupati, J. Narayan, F. Hunte, Room temperature ferromagnetism in epitaxial Cr2O3 thin films grown on r-sapphire, J. Appl. Phys. 117 (2015) 1–5.

https://doi.org/10.1063/1.4896975.

[5] S.P. Pati, N. Shimomura, T. Nozaki, T. Shibata, M. Sahashi, Néel temperature of Cr_2O_3 in Cr_2O_3/Co exchange-coupled system: Effect of buffer layer, J. Appl. Phys. 117 (2015) 17D137. https://doi.org/10.1063/1.4917263.

[6] S.Y. Jeong, J.B. Lee, H. Na, T.Y. Seong, Epitaxial growth of Cr2O3 thin film on Al 2O3 (0001) substrate by radio frequency magnetron sputtering combined with rapid-thermal annealing, Thin Solid Films. 518 (2010) 4813–4816. https://doi.org/10.1016/j.tsf.2010.01.046.

[7] T.C. Kaspar, S.E. Chamberlin, S. a. Chambers, Surface structure of ??-Cr2O3(0001) after activated oxygen exposure, Surf. Sci. 618 (2013) 159–166. https://doi.org/10.1016/j.susc.2013.09.005.

[8] S. Khamlich, Z.Y. Nuru, A. Bello, M. Fabiane, J.K. Dangbegnon, N. Manyala, M. Maaza, Pulsed laser deposited Cr2O3 nanostructured thin film on graphene as anode material for lithium-ion batteries, J. Alloys Compd. 637 (2015) 219–225. https://doi.org/10.1016/j.jallcom.2015.02.155.

[9] T. Ashida, M. Oida, N. Shimomura, T. Nozaki, T. Shibata, M. Sahashi, Isothermal electric switching of magnetization in Cr2O3/Co thin film system, Appl. Phys. Lett. 106 (2015) 101–106. https://doi.org/10.1063/1.4916826.

[10] M. Gomi, Epitaxial Growth of α-Fe2O3 and Cr2O3 Sputtered Films on Garnet, J.Phys.IV Fr. 7 (1997) 481–482. https://doi.org/10.1051/jp4.

[11] A. Stierle, T. Koll, H. Zabel, Structure and defects of epitaxial overlayers on Cr(110),

Phys. Rev. B - Condens. Matter Mater. Phys. 58 (1998) 5062–5069. https://doi.org/10.1103/PhysRevB.58.5062.

[12] K. Asami, K. Hashimoto, The X-ray photo-electron spectra ofseveral oxides of iron and chromium, Corros. Sci. 17 (1977) 559–570. https://doi.org/10.1016/S0010-938X(77)80002-4.

[13] T. Wang, J. Shi, W. Yuan, Z. Zhang, X. Ma, W. Xing, T. Su, P. Gao, Y. Chen, Q. Song, W. Han, Crystal Structure Manipulation of the Exchange Bias in an Antiferromagnetic Film, Sci. Rep. 6 (2016) 1–8. https://doi.org/10.1038/srep28397.

[14] M.W. Herdiech, X. Zhu, M.D. Morales-Acosta, F.J. Walker, E.I. Altman, The modification of ferroelectric LiNbO3(0001) surfaces using chromium oxide thin films, Phys. Chem. Chem. Phys. 17 (2015) 9488–9498. https://doi.org/10.1039/c4cp05875e.

[15] A. Lodesani, A. Picone, A. Brambilla, D. Giannotti, M.S. Jagadeesh, A. Calloni, G. Bussetti, G. Berti, M. Zani, M. Finazzi, L. Duo, Graphene as an Ideal Bu ff er Layer for the Growth of High-Quality Ultrathin Cr 2 O 3 Layers on Ni(111), (2019) 3–9. https://doi.org/10.1021/acsnano.8b09588.

[16] T. Asada, K. Nagase, N. Iwata, H. Yamamoto, Crystal Growth of Magnetoelectric Cr 2 O 3 Thin Film on Sapphire and SrTiO 3, Jpn. J. Appl. Phys. 47 (2008) 546. http://stacks.iop.org/1347-4065/47/i=1S/a=546.

[17] T. Kolodiazhnyi, A. Petric, The Applicability of Sr-deficient n-type SrTiO 3 for SOFC Anodes, J. Electroceramics. 15 (2005) 5–11.

[18] L.E. Rehn, Ion beams in high - temperature superconductivity research, Nucl. Instruments

Methods Phys. Res. Sect. B Beam Interact. with Mater. Atoms. B64 (1992) 161–168.

[19] I. Horcas, R. Fernández, J.M. Gómez-Rodríguez, J. Colchero, J. Gómez-Herrero, A.M. Baro, WSXM: A software for scanning probe microscopy and a tool for nanotechnology, Rev. Sci. Instrum. 78 (2007). https://doi.org/10.1063/1.2432410.

[20] J. Rubio-Zuazo, P. Ferrer, a. López, a. Gutiérrez-León, I. da Silva, G.R. Castro, The multipurpose X-ray diffraction end-station of the BM25B-SpLine synchrotron beamline at the ESRF, Nucl. Instruments Methods Phys. Res. Sect. A Accel. Spectrometers, Detect. Assoc. Equip. 716 (2013) 23–28. https://doi.org/10.1016/j.nima.2013.03.019.

[21] V. Pishchik, L.A. Lytvynov, E.R. Dobrovinskaya, Sapphire, 2009. https://doi.org/10.1007/978-0-387-85695-7.

[22] A. Serrano, J. Rubio-Zuazo, J. López-Sánchez, I. Arnay, E. Salas-Colera, G.R. Castro, Stabilization of Epitaxial α-Fe2O3 Thin Films Grown by Pulsed Laser Deposition on Oxide Substrates, J. Phys. Chem. C. 122 (2018) 16042–16047. https://doi.org/10.1021/acs.jpcc.8b02430.

[23] J.F.M. C.D. Wagner, W.M. Riggs, L.E. Davis, Handbook of X-ray Photoelectron Spectroscopy, first ed., Perkin-Elmer Corporation, Minnesota, 1979, 1979.

[24] I. Pollini, Splitting of core-level lines in photoemission spectra of transition metal compounds, Philos. Mag. 85 (2005) 2641–2652. https://doi.org/10.1080/14786430500154372.

[25] I. Ikemoto, K. Ishii, S. Kinoshita, H. Kuroda, M.A. Alario Franco, J.M. Thomas, X-ray photoelectron spectroscopic studies of CrO2 and some related chromium compounds, J.

Solid State Chem. 17 (1976) 425–430. https://doi.org/10.1016/S0022-4596(76)80012-6.

[26] V.R. Galakhov, M. Demeter, S. Bartkowski, M. Neumann, N.A. Ovechkina, E.Z. Kurmaev, N.I. Lobachevskaya, Y.M. Mukovskii, J. Mitchell, D.L. Ederer, Mn 3s exchange splitting in mixed-valence manganites, Phys. Rev. B. 65 (2002) 113102. https://doi.org/10.1103/PhysRevB.65.113102.

[27] J.C. Carver, G.K. Schweitzer, T.A. Carlson, Use of X-Ray Photoelectron Spectroscopy to Study Bonding in Cr, Mn, Fe, and Co Compounds, J. Chem. Phys. 57 (1972) 973–982. https://doi.org/10.1063/1.1678348.

[28] K. Okada, V. Kinsinger, R. Zimmermann, S. Hüfner, Photoemission from Cr 2p and 3s Levels of CrF2, J. Phys. Soc. Japan. 63 (1994) 2410–2415. https://doi.org/10.1143/JPSJ.63.2410.

[29] S.P. Kowalczyk, N. Edelstein, F.R. McFeely, L. Ley, D.A. Shirley, X-ray photoemission spectra of the 4d levels in rare-earth metals, Chem. Phys. Lett. 29 (1974) 491–495. https://doi.org/10.1016/0009-2614(74)85076-1.

[30] J.H. Van Vleck, The dirac vector model in complex spectra, Phys. Rev. 45 (1934) 405–419. https://doi.org/10.1103/PhysRev.45.405.

Acknowledgements

The ESRF, MCIU and CSIC are acknowledged for the provision of synchrotron radiation facilities under Project No. PIE 2010-6-OE-013. This work has received financial support from Ministerio de Economía y Competitividad (Spain) under Project No. MAT2017-82970-C2-R and MAT2017-82970-C2-2-R. The microscopy works was conducted in the Laboratorio de Microscopías

Avanzadas (LMA) at Instituto de Nanociencia de Aragón (INA)-Universidad de Zaragoza. The authors acknowledge the LMA-INA for offering access to their instruments and expertise. A. Prados would like to acknowledge the postdoctoral fellowship granted by Comunidad de Madrid and the European Union [PEJD-2016/IND-2233] and the use of facilities of Instituto de Sistemas Optoelectrónicos y Microtecnología (ISOM-UPM).